Ceramics-Silikáty 65 (3), 215-223 (2021)
www.ceramics-silikaty.cz doi: 10.13168/cs.2021.0021

STRUCTURAL CHARACTERISATION OF ASPHALT-RICE HUSK SILICA COMPOSITES

#SIMON SEMBIRING*, AGUS RIYANTO*, IQBAL FIRDAUS*, JUNAIDI*, ENDAH AYU NINGTIAS*, RUDY SITUMEANG**

*Department of Physics, Faculty of Mathematics and Natural Sciences, University of Lampung, Jl. Prof. Soemantri Brojonegoro, Bandar Lampung, 35145, Indonesia
**Department of Chemistry, Faculty of Mathematics and Natural Sciences, University of Lampung, Jl. Prof. Soemantri Brojonegoro, Bandar Lampung, 35145, Indonesia

#E-mail: simonsembiring2@gmail.com

Submitted February 24, 2021; accepted May 18, 2021

Keywords: Rice husk, Silica, Asphalt, Microstructure, Thermal, Structure

This research characterises the structure and micro-structure of asphalt-silica composites heated to a temperature of 150 °C, as well as their physical and mechanical properties. The asphalt and silica mass ratios were varied into 10:90, 15:85, 20:80, 25:75, 30:70 and 35:65. The characterisation of the asphalt-silica composite was performed using Fourier Transform Infrared (FTIR), X-ray Diffraction (XRD), and Scanning Electron Microscopy (SEM). The results of the XRD studies show that the main phases are amorphous silica and carbon, which are linked to the functional groups of silicon hydroxide, silicon dioxide and alkanes. The other results show that the reduced water absorption, compressive strength, and density are caused by the increased porosity and swelling thickness with an increasing amount of the added asphalt. Asphalt-silica composites with asphalt addition from 10 to 20 % experience insignificant changes in compressive strength, water absorption, and swelling thickness. These results prove that asphalt has a significant impact on the phase of silica, making it have the potential to replace light steel roofing devices.

INTRODUCTION

Rice husks, as a biomass waste, are available in abundance and this sustainable waste is beneficial to use due to its SiO_2 content that makes it a cost-effective alternative source of silica. Earlier studies [1-7] proved that rice husks have the potential to be a source of silica with high purity, activity, and amorphous level, and that it can be prepared in sols due to its high solubility in alkali solutions. The silica obtained from rice husk has also been successfully used as an alternative to produce nanosilica [8-10], ferrisilicate [11], forsterite [12-13], cordierite [14], silica-asphalt composite [15-16] and mullite [17]. There are also other research studies using silica from rice husks as a distilled vegetable oil for medicine, detergents, adhesives, ceramics, pesticides [18-19], energy-saving agents [20], and catalysts [21-22].

Silica can be used to produce an asphalt composite with a desired performance because of its strong thermal stability, large specific area, high reactivity, good dispersion and adsorption ability. It has great advantages in improving the temperature performance, fatigue, water stability, elastic stretching, and asphalt temperature susceptibility [23-29]. Some researchers have carried out low temperature bending tests on asphalt matrix mixtures [30]. They found that the addition of silica improves the low temperature performance and increases the shrinkage coefficient of these mixtures. In addition, asphalt modifications using 2 - 4 % silica show increases in the softening and viscosity points as well as a reduction in the penetration rate, resulting in a stiff behaviour and high modulus [31]. A mixture of 7 % asphalt with silica indicates that the asphalt resistance to the asphalt stability increases [22], and the resistance to ageing and fatigue cracking also increases [23] with the use of 4 and 6 % silica. At the same time, addition of 1 and 2 % silica increases the soft point and asphalt hardness, as well as providing high resistance to rutting deformations [32].

Asphalt is a unique viscoelastic solid at room temperature [33], consisting of weak chemical bonds that are easily modified by temperature. It is also a complex alloy of elastic compounds with a relatively low hydrogen-carbon ratio and high boiling point, which is highly dependent on the loading time and temperature [34-35]. These characteristics mean that asphalt is generally used as an aggregate binder, such as for the construction of flexible pavements, buildings and roofing materials. Heat treatment allows asphalt to turn into a liquid adhesive and is easily mixed with other materials. During the cooling process, asphalt becomes waterproof, sticky,

and strong. However, temperature susceptibility limits the use of asphalt. This is where modification comes into play. Several kinds of fibre forms have the potential to be used in conjunction with asphalt, including glass, carbon, and polymers. Asphalt mixtures tend to be more resistant to low temperature cracking and permanent deformation [36], and have high a tensile strength with the addition of fibres [37]. Adding rubber powder and a transformer increases the penetration point and hardness of asphalt [38], and cement can improve the modulus of stiffness, rutting resistance, resistance to moisture, and asphalt fatigue [39]. Several other researchers have used various polymers for rubber-based blends [40-42], fibres and scrap fibres [35,43], and nanocomposite polymers and have observed different mechanical properties of asphalt [44-45].

This research aims to figure out the structure and micro-structure of asphalt-silica composites, as well as their physical and mechanical properties. Emphasis has been placed on the effect of the asphalt-silica ratio to the structure, and micro-structure of the asphalt-silica composites**.** Detailed information on some features of the asphalt-silica composite has been obtained from analyses using FTIR, XRD, and SEM. Furthermore, several physical and mechanical properties of the asphalt-silica composites were investigated.

EXPERIMENTAL

The asphalt used in this experiment was obtained from a refinery in Buton, Southeast Sulawesi province in Indonesia, while the modifier is a rice husk silica. The 5 % NaOH and 10 % HNO_3 were purchased from Aldrich and the absolute alcohol (C_2H_5OH) was purchased from Merck. The synthesis of the asphalt-silica composite consists of two steps; (i) silica extraction, and (ii) asphalt and rice husk silica mixture with different amounts of asphalt and silica. The silica was extracted from the rice husk with the technique used in a previous study [12]. 10 % HNO_3 was gradually added to the acquired sol solution to turn the sol into a real gel. The gel was then heated in an oven at 110 °C for 10 hours and pulverised until it became a powder and was sifted using a 200 Millipore screen. The asphalt-silica composite synthesis was performed for a suitable mixture of asphalt and silica. A total of 100 g of the lumped asphalt was diluted under thermal treatment at 100 °C and mixed with the silica powder using a shear mixer at 125 rpm for 6 hours. The next process was to get a solid asphalt-silica composite, a certain amount of asphalt and silica were mixed according to the mass ratios of 10:90, 15:85, 20:80, 25:75, 30:70 and 35:65. These mixtures were then pressed in a cylindrical metal die at 2×10^4 N·m^{-2}, which was then calcined at 150 °C using the technique used in previous studies [15], using a programmed temperature increase of 3 °C·min^{-1} for 5 hours. The asphalt and silica reactions were observed using FTIR, XRD, and SEM. Meanwhile, the FTIR spectrum was conducted with a Merk Perkin Elmer. These samples were then milled using an analytical grade KBr. The X-ray diffraction pattern was recorded using an automatic Shimadzu XD-610 with a copper radiation source (λ = 1.5406 nm). The XRD spectrum was collected in the 2θ range (10 - 100°), calculating 1 second with 0.02 step size. The microstructure change and chemical element analyses were observed by a SEM Philips-XL coupled with energy dispersive spectrometry (EDS). Afterwards, the bulk density and porosity were measured [46], the absorption of water and thickness of swelling were observed in accordance with JIS A 5908 [47]. Finally, the compression strength was measured using an MTS Landmark 100 kN. The compressive strength was calculated using σ = F/A (F = Force (Newton) and A = Surface area (m^2)). The dimensions of the measured sample for the compressive strength were 0.005 m thick and 0.02 m in diameter.

RESULTS AND DISCUSSION

Structural properties of asphalt-silica composite

The interaction mechanism between the asphalt and the rice husk silica was investigated using a FTIR spectrometer. The FTIR spectrum of the samples is shown in Figure 1a-h. The FTIR spectrum of asphalt is shown in Figure 1a and the FTIR spectrum of silica is shown in Figure 1b, while the FTIR spectrum of the samples with the different asphalt contents is shown in Figure 1c-h.

Figure 1a shows the presence of three high peaks at 2928, 1723, and 1266 cm^{-1}, and followed by other peaks at 962, 752, and 693 cm^{-1}. The peaks at 2928 and

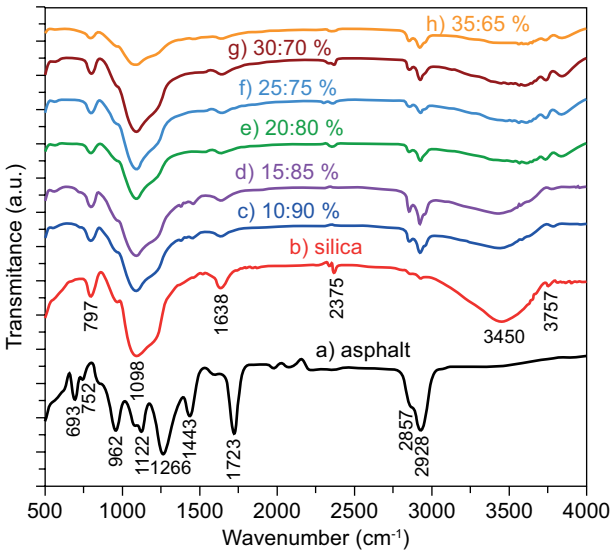

Figure 1. FTIR characteristics of the asphalt-silica composites with a different asphalt and silica mass ratio.

1266 cm^{-1} present the function of the O–H characteristic group of the carboxylic acids and that of C–H from the alkanes, while the peak at 1723 shows the vibrations of the carbonyl group C = O [15]. Others strong peaks are located at 962, 752, and 693 cm^{-1}, which are related to the bending vibrations of C–H in the phenyl. The silica sample (Figure 1b) reveals the existence of a broad band centred around the 3450 cm^{-1} region, which is attributed to the stretching vibration of the hydroxyl (–OH) group of silanol (SiOH). The existence of the Si–OH bond is supported by a weak band centred around 1098 cm^{-1}, and the presence of the adsorbed water molecules is supported by the absorption band centred around 1638 cm^{-1}, which is attributed to the bending vibration of the O–H bond. The two characteristic bands at 1098, and 797 cm^{-1} are attributed to the asymmetric stretching vibration, symmetric stretching vibration, and bending vibration of the Si–O–Si.

For the samples with 10 % and 15 % asphalt (Figure 1c-d), the presence of functional groups is almost the same as the silica functional groups in Figure 1b, namely the O–H, Si–OH and C–H groups. However, in Figure 1c-d, the strong peaks appear at 797, 2857, and 2928 cm^{-1} are caused by the asphalt-induced C-H vibrations, which may be characteristic of the O–H vibrations of the carboxylic acid and the C–H vibrations of the alkanes, as was also found in previous studies [48-49]. The obvious effect of adding asphalt to the functional groups of the sample is shown in Figure 1e-h**.** A significant influence can be seen with the appearance of the peaks associated with the hydroxyl function around 3450 cm^{-1}, indicating a reaction between the asphalt and silica during the asphalt addition process. The most obvious change can be seen with the peak decrease associated with $Si(OH)_4$, which includes the interaction between the asphalt and the silica. The decrease in this band is caused by the vibrations of the SiO tetrahedral structure and the change in intensity indicates the disorientation of the asphalt as a result of the interconnection of the asphalt molecules and the silica. This is also supported by a decrease in the intensity of the O–H bond band due to the release of water molecules and OH species through the breakdown of the asphalt**.** As a result, the intensity of the absorption bands at 797, 1638, and 1098 cm^{-1} decreased which was followed by an increase in the bands at 2857 and 2928 cm^{-1}. The results from the samples also show a gradual reduction in the absorption peak at 3450 cm^{-1} to an increase with the 30 % asphalt and its practical disappearance at 35 %. This indicates that Si(OH) reacts with asphalt. However, the addition of asphalt appears to affect the intensity of the chemical group of the silica, and hence, the overall material performance. Thus, it is concluded that silica undergoes an inter-bond change with the addition of asphalt. In the absence of a new peak appearing in the sample curve, it is assumed that no new functional group formation is produced in the samples.

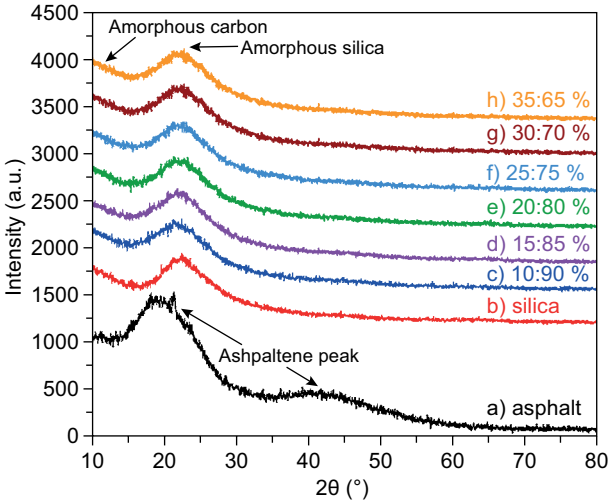

Figure 2. FXRD characteristics of the asphalt-silica composite with a different asphalt and silica mass ratio.

Samples were then analysed using XRD to understand the reaction process of the asphalt and the silica. Figure 2a shows the spectrum of the asphalt and Figure 2b-g presents the patterns of the samples with the different asphalt contents.

The diffraction patterns presented in Figure 2a reveal the presence of two wide peaks of about 23.20° and 42.50° of 2θ indicating the formation of asphaltenes' crystals which occur due to condensed aliphatic chains or saturated rings, while the formation of multi-layered graphene takes place by the staging aromatic molecules present in the asphaltenes' structure. This phenomenon was also found in previous studies. [15]. The diffraction pattern of the sample with the addition of 10 % asphalt (Figure 2b) explains the presence of the amorphous crystalline phase located at about 18 - 30° of the 2θ value. In more detail, the amorphous crystalline phase of the sample shows crystals of asphaltene (carbon) and silica, found in the diffraction pattern of the samples. These indicate that some of the hydroxide components accumulate in the sample, as shown in the FTIR results (Figure 1c-h). Furthermore, the intensity of the amorphous silica structure with a peak of 2θ at 21.8° decreased with the addition of asphalt (Figure 2c-h), indicating that the asphalt does not react with the silica. In addition, the decrease in the intensity of the amorphous silica is assumed to result in a very strong bond between the asphalt and the silica molecules through London dispersion forces, without the formation of new structures. The existence of bonds between the asphalt and silica molecules is supported by the presence of the Si–OH and C–H groups (Figure 1c-h) and the detection of carbon and silica elements (Table 1).

Figure 3 presents the SEM inspections of the asphalt-silica composite after being calcined to a temperature of 150 °C and Table 1 shows the chemical compositions of the samples. As shown in Figure 3 and Table 1, the surface morphologies of the samples are characterised by the presence of particles with different

grain sizes and distributions, as well as detection of the major elements C, Si and the minor elements Na and S, as supported by previous studies [15]. The detection of C and Si indicates that the asphalt and silica do not react, so there is no new phase formation, as shown by the XRD results in Figures 2b-c. The microstructure of the samples with a 10 % asphalt content (Figure 3a) do not show any major different characteristics, in comparison with the 15 % asphalt content (Figure 3b). The surface of both samples is characterised by smaller asphaltenic phases that disperse into several large grains of silica particles. The asphalt reacts with the silica, so that the pore size becomes larger as the asphalt coagulates, supported by the presence of carbon and silica, as presented in the XRD results (Figures 2b-c). Figures 3c-f shows that the surface morphology at a higher asphalt content of about 20 %, 25 %, 30 % and 35 % accumulates with an inhomogeneous shape and size of the asphaltenic structures that cover large grains of silica**.** It can be concluded that as the asphalt content increases, more hydroxide products are produced, and the pores are filled with the asphalt. The interaction of the asphalt and silica increases the size and changes the shape of the particles. These phenomena suggest that silica and asphalt particles interact strongly and uniformly. The modified asphalt does not form new structures, but the silica in the asphalt can change the physical and mechanical properties of the asphalt. All the samples were marked by an initial low crystallisation of the silica, which indicates the formation process of the structural asphalt-silica composite**.** In this study, the properties of asphalt-silica composite are mainly determined by the asphalt phase, that is, by the type of the component and the amount of the asphalt. It was observed that the proper amount of the asphalt mixture mixed with silica is 10 to 20 %.

The elemental analysis of the asphalt-silica composite is given in Table 1. The analysis shows the significance of adding asphalt compared to the silica for the composition of the silica and carbon. As presented in Table 1, an amount of carbon (34.33 %) is found from a 10% asphalt addition. This figure increases to 49.64 % with the addition of up to 35 % asphalt. Meanwhile, samples with an asphalt addition of 10 % contained 23.46 % and decreased to 14.72 % with an asphalt addition of up to 35 %. The SEM image also shows that the sample has high viscosity with an increase in the asphalt to 35 %.

Table 1. Elemental analysis of the asphalt-silica composite.

Asphalt (%)	Oxygen O (wt. %)	Carbon C (wt. %)	Silicon Si (wt. %)	Sulfur S (wt. %)	Sodium Na (wt. %)
10	39.38	34.33	23.46	0.60	2.23
15	40.26	38.81	18.06	0.98	1.99
20	38.44	41.59	16.90	1.31	1.76
25	39.14	42.13	15.11	1.24	2.28
30	40.54	43.28	14.83	0.98	1.37
35	32.91	49.64	14.72	1.45	1.28

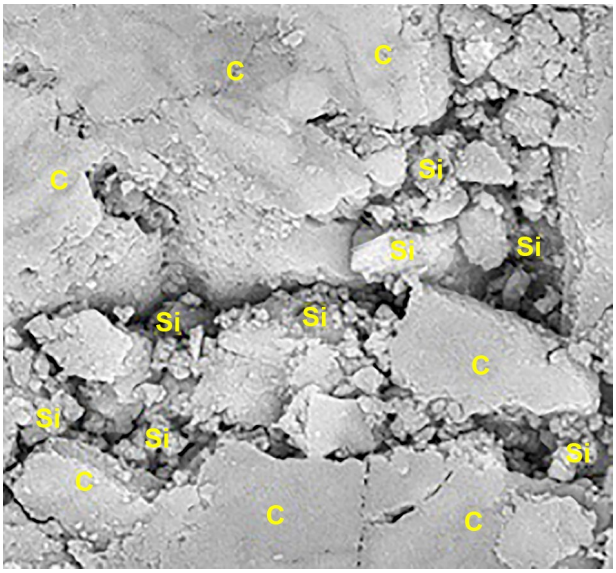

a) 10:90 %

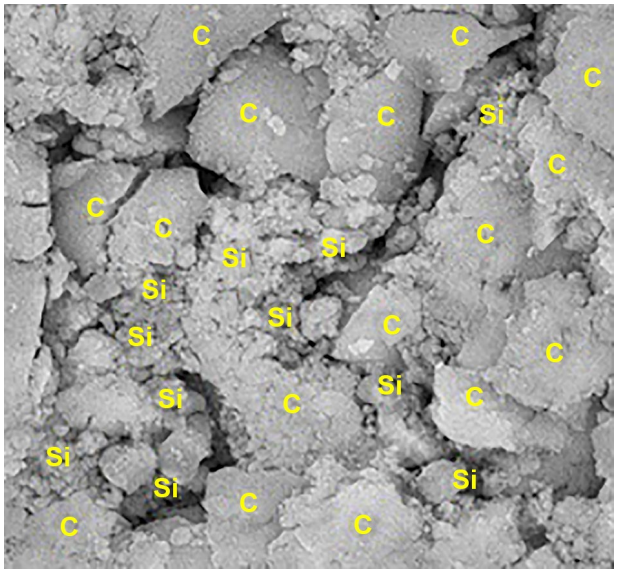

b) 15:85 %

Figure 3. SEM characteristics of the asphalt-silica compo-site with a different asphalt and silica mass ratio: a) 10:90 %, b) 15:85 % (legend: C = Carbon, Si = Silica). *(Continue on next page)*

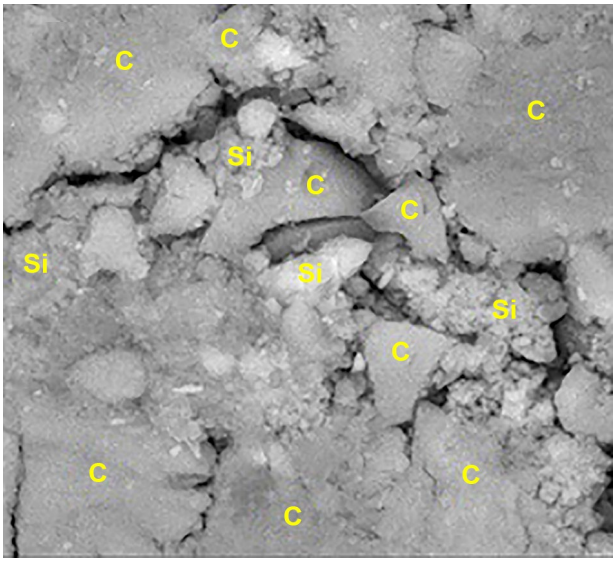

c) 20:80 %

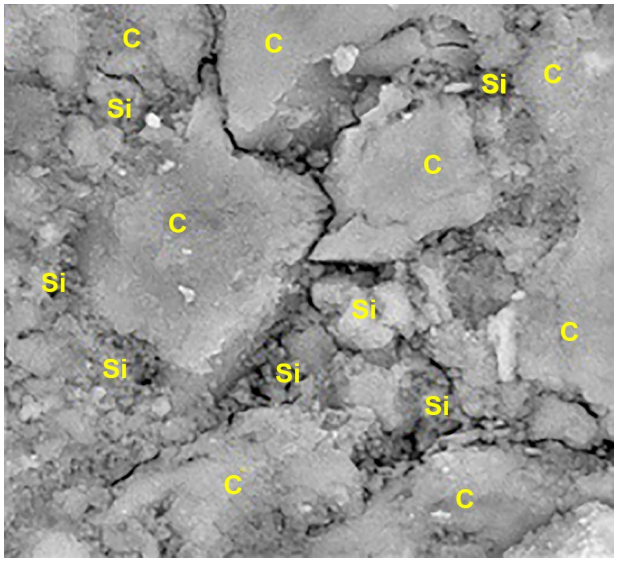

d) 25:75 %

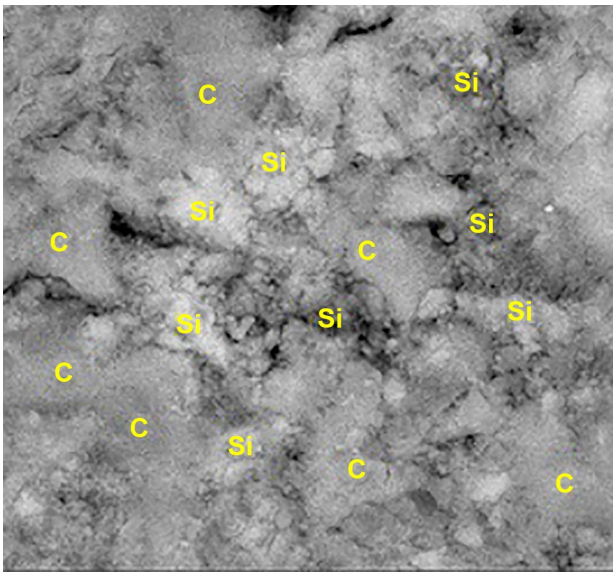

e) 30:70 %

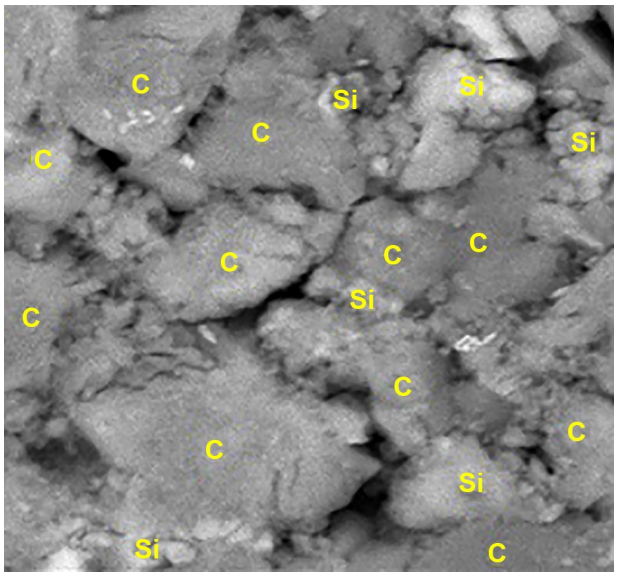

f) 35:65 %

Figure 3. SEM characteristics of the asphalt-silica composite with a different asphalt and silica mass ratio; c) 20:80 %, d) 25:75 %, e) 30:70 %, f) 35:65 % (legend: C = Carbon, Si = Silica).

Physical properties of the asphalt-silica composite

The change in the density and porosity with the increasing asphalt ratio is shown in Figure 4. These results showed that the porosities of the samples increased slowly with the addition of asphalt to 25 % and increased sharply with the addition of asphalt up to 35 % (Figure 4a). The increase in the porosity with the addition of asphalt up to 35 % was clearly seen as a result of the increase in the carbon content (Table 1). This result implies that the non-uniformity in the pore size leads to an increased porosity and permeability, and hence, a softer matrix, and also implies that the formation of pozzolans occurs with the presence of the asphalt around the silica. Meanwhile, the samples' densities decrease sharply with the asphalt addition to 25 % and decrease slowly with an asphalt addition to 35 %. As can be seen in Figure 4b, the densities decreased from 3.95 to 3.05 g·cm^{-3} as the asphalt content increased from 10 to 20 %, and the densities slowly decreased with asphalt content from 20 to 30 %, and they reached the value of 2.35 g·cm^{-3} at an asphalt content of 35 %. This phenomenon is caused by a decrease in the silica, as shown in Table 1. Increasing the asphalt content seems to increase the propagation of the pores in the matrix, resulting in a sudden increase in the porosity, as shown in Figure 4a. The decrease in the sample density corresponds to the decrease in the silica and increase in the carbon, as shown in Table 1**.** From the physical properties, it can be seen that the increase in the porosity is evident with pores of different shapes and sizes on the sample surface. In addition, this phenomenon also

occurs due to the carbon agglomeration around the silica particles and the increase in the carbon with the addition of the asphalt. It was also observed that the asphalt molecules, as binders, have self-binding properties, causing the formation of pores, thereby increasing the number of inhomogeneous pore nucleation sites in the asphalt-silica structure.

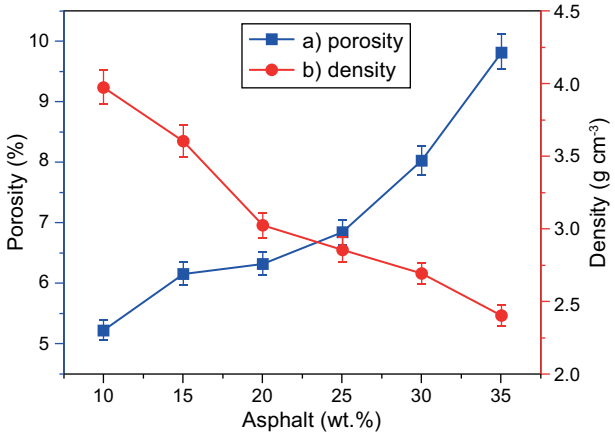

Figure 4. The change in porosity (a) and density (b) of the asphalt-silica composite with a different asphalt and silica mass ratio.

The compressive strength-displacement curves of the samples with the different asphalt contents are presented in Figure 5. The results indicate that the compression strength of the asphalt composite decreased with an increasing asphalt content. As shown in Figure 5, the compressive strength for all the samples does not change until a displacement of 0.4 mm. Furthermore, samples with an asphalt content of 10, 15, 25, 30, and 35 % experienced the maximum increase in the compressive strength with a displacement of 1.5 mm, while the sample with the addition of 20 % asphalt experienced the maximum compressive strength with a displacement of 2 mm. This trend implies that the sample density decreases as a result of an increase in the amount of asphalt and carbon. Briefly, these findings suggest that the compressive strength of the sample corresponds to the changes in the porosity and density produced in this study, which are more clearly shown in Figure 6. The results indicate that the compressive strength of the asphalt-silica composite decreased noticeably with an increased asphalt content in the sample.

It can be seen from Figure 6 that the compressive strength increased with the change in the asphalt addition from 10 to 15 %. The increase in the compressive strength of the sample with the 15 % asphalt addition is due to the high binding ability of the asphalt to the silica, which fills the spaces among the silica grains. The compressive strength decreased sharply with the addition of asphalt up to 35 %, followed by a large increase in the porosity and a decrease in the density, as shown in Figure 4. This phenomenon is due to the small specific surface of the silica where the ability of the asphalt to bind the silica is weak to fill the spaces among the various silica grains. The compressive strength increased smoothly when increasing the asphalt content from 10 to 15 % and reached a value of 46.5 MPa, and decreased when increasing the asphalt content up to 35 % and reached a value of 25.6 MPa. The results also clearly show that the highest asphalt composite compressive strength is obtained when using an asphalt addition of 15 %. A reduction in the compressive strength starts from an asphalt content at 15 to 35 % due to the weak bond between the asphalt and silica particles. These characteristics indicate that the asphalt-silica composite becomes less fused and less dense as a result of the decrease in the amount of silica and the increase in the amount of carbon (Table 1). Obviously, the results of this

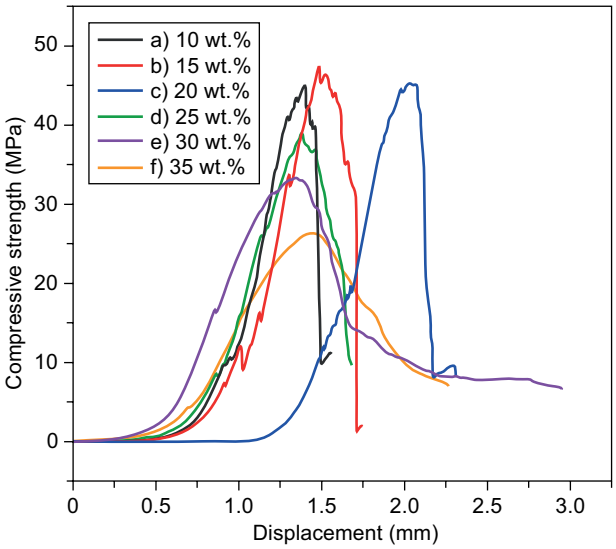

Figure 5. Compressive strength-displacement curves of the samples with the different asphalt contents.

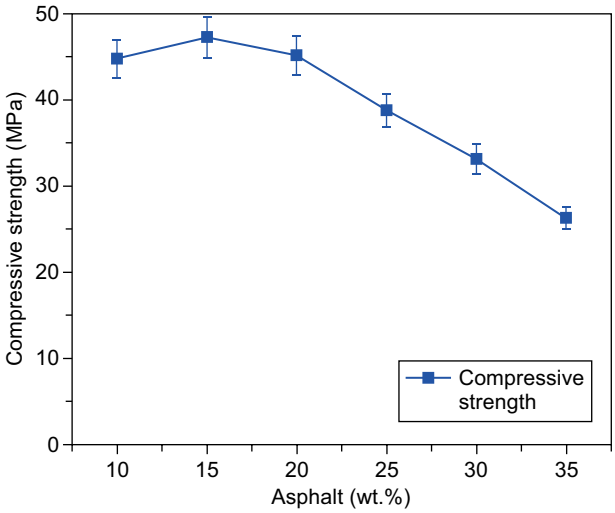

Figure 6. Variation in the compressive strength of the asphalt-silica composite with the different asphalt contents.

study strongly reveal that the changes in the compressive strength are in line with the changes in the density and porosity (Figures 4a and b). The parameters of the density, porosity and structural characteristics greatly affect the compressive strength value. In addition, the homogeneity, size and distribution of the particles largely determine the compressive strength value.

Figure 7 shows the changes in the water absorption and swelling thickness of the asphalt-silica composite prepared with the different asphalt contents. Figure 7a shows that the water adsorption of the samples increases slowly from an asphalt content of 10 to 20 %, and decreases up to 25 %, and relatively increases up to 35 %. It can also be seen that the water absorption for an asphalt increase from 10 to 20 % is greater than for an asphalt increase from 20 to 35 %. Figure 7a shows that, overall, an increasing asphalt content reduces water absorption in the mixture. The full saturation of the samples during this test causes a reduction in the amount of water absorption that, in turn, is due to the filling of the silica voids (including pores and entrapped air voids) with asphalt, and the reduction of the entrapped air voids inside the silica. In contrast to the water absorption, the swelling thickness of the samples increases with an increase in the asphalt content, as shown in Figure 7b. The increased swelling thickness with the addition of the asphalt is attributed to a suitable carbon and silica ratio (Table 1), and the formation of some micro-cavities is probably influenced by the lack of bonding between the silica and the asphalt. This phenomenon reveals that the swelling thickness increases with an increasing asphalt content until it reaches a certain value, where it no longer occurs. This may also be due to the reduced spread and interface bonding between the asphalt and the silica, as shown in Figure 3. These profiles suggest that the swelling thickness is due to the presence of the silica structure and low viscosity of the asphalt-silica composite samples. These results also indicate that the water absorption and swelling thickness can be reduced by adjusting the number and formation of the silica particles, it will be useful in assessing the significance of the material for its application to suit various desires. Other important aspects in designing the water absorption and swelling thickness are the size, and even the distribution of silica the particles and asphalt arrangement according to the microstructure, as shown in Figure 3.

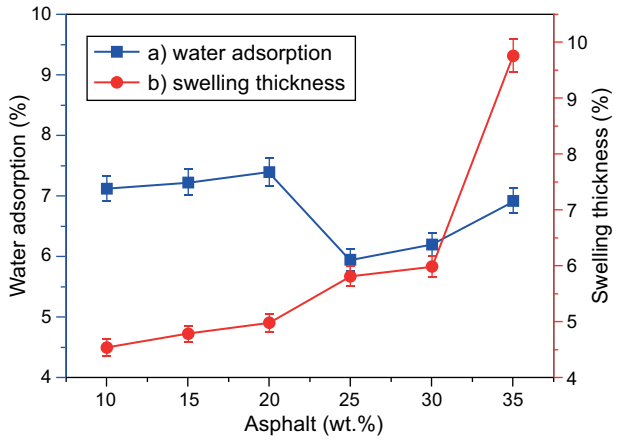

Figure 7. Water absorption and thickness swelling of the asphalt-silica composite with the different asphalt contents.

CONCLUSIONS

The present investigation revealed some of the reactions and physical properties of the asphalt-silica composites. The XRD and FTIR studies show that the asphalt-silica composites' phase with the additional asphalt does not change the amorphous silica phase. The surface morphology of the asphalt-silica composites results in the formation of large groups with different pore shape distributions on the surface. The microstructure of the asphalt-silica composites shows that the dispersed asphalt binds the silica with inhomogeneous particle sizes on the sample surface. The addition of asphalt can reduce the water absorption and density. The asphalt-silica composites with the additional asphalt of 10 to 20 % experience insignificant changes in the compressive strength, water absorption, as well as the swelling thickness so that they can be used as an alternative roofing material to lightweight steel roofing.

Acknowledgments

The authors wish to thank the Ministry of Research, Technology, and Higher Education of the Republic of Indonesia for the research funding provided through Superior Research university Grant No: 062/SP2H/LT/DRPM/2021 and DIPA Unila Program for 2021

REFERENCES

1. Rafieel E., Shahebrahimi S., Feyzil M., Shaterzadeh M. (2012): Optimization of synthesis and characterization of nanosilica produced from rice husk (a common waste material). *International Nano Letters, 2(1),* 1-8. doi: 10.1186/2228-5326-2-29
2. Hassan A. F., Abdelghny A. M., Elhadidy H., Youssef A. M. (2014): Synthesis and characterization of high surface area nanosilica from rice husk ash by surfactant-free sol-gel method. *Sol-Gel Science and Technology, 69*, 465-472. doi: 10.1007/s10971-013-3245-9
3. Alvarez J., Lopez G., Amutio M., Bilbao J., Olazar M. (2014): Upgrading the rice husk char obtained by flash pyrolysis for the production of amorphous silica and high quality activated carbons. *Biosource Technology, 170*, 132-137. doi: 10.1016/j.biortech.2014.07.073
4. Gu S., Zhou J., Luo Z. (2015): Kinetic study on the preparation of silica from rice husk under various pretreatments. *Thermal Analysis Calorimetri, 119*; 2159-2169. doi: 10.1007/s10973-014-4219-z

5. Sankar S., Sharma S. K., Kaur N., Lee B., Kim D. Y., Lee S., Jung H. (2016): Biogenerated silica nanoparticles synthesized from sticky, red, and brown rice husk ashes by chemical method. *Ceramics International, 42*, 4875-4885. doi: 10.1016/j.ceramint.2015.11.172
6. Le Nghiem A. T., Lai Thi K. D., Le Doan T.H., Nguyen Q. H., Dang V. P., Bui D.D. (2017): Preparation and characterization of nanosilica from rice husk ash by chemical treatment combined with calcination. *Vietnam Chemistry International Edition, 55 (4),* 455-459. doi: 10.15625/2525-2321.2017-00490
7. Feng Q., Chen K. D., Ma D. (2018): Synthesis of high specific surface area silica aerogel from rice husk ash via ambient pressure drying. *Colloid and Surface, A539*, 399-406. doi:10.1016/j.colsurfa.2017.12.025
8. Sarangi M., Bhattacharyya S., Behera R. C. (2009): Effect of temperature on morphology and phase transformations of Nano crystalline silica obtained from rice husk. *Phase Transitions, 82(5)*, 377-386. doi: 10.1080/01411590902978502
9. Soltani N., Bahrami A., Pech-Canul M. I., and Gonzales. (2015): Review on the physiochemical treatments of rice husk for production of advanced materials. *Chemical Engineering, 264*, 899-935. doi: 10.1016/j.cej.2014.11.056
10. Bathla A., Narulal C., Chauhan R. P. (2018): Hydrothermal synthesis and characterization of silica nanowires using rice husk ash: an agricultural waste. *Material Science Material in Electronic, 29*, 6225-6231. doi: 10.1007/s10854-018-8598-y
11. Bhagiyalakshmi M., Auradha R., Palanichamy M., Jang H. T. (2010): Dexterous template-free synthesis of ferrisilicate with MFI morphology using rice husk ash. *Journal of Non Crystalline Solids, 356 (23-24)*, 1204-1209. doi: 10.1016/j.jnoncrysol.2010.04.017
12. Sembiring S., Riyanto A., Simanjuntak W., and Situmeang R. (2017): Effect of MgO–SiO_2 Ratio on the Forsterite (Mg_2SiO_4) Precursors Characteristics Derived from Amorphous Rice Husk Silica. *Journal of Oriental Chemistry, 33(4)*, 1828-1836. doi: 10.13005/ojc/330427
13. Hossain S. K. S, Mathur L., Singh P., Majhi M. R. (2017): Preparation of forsterite refractory using highly abundant amorphous rice husk silica for thermal insulation. *Asian of Ceramic Society, 5*, 82-87. doi: 10.1016/j.jascer.2017.01.001
14. Sembiring S., Simanjuntak W., Situmeang R., Riyanto A., and Sebayang K. (2016): Preparation of Refractory Cordieirite Using Amorphous Rice Husk Silica for Thermal Insulation Purposes. *Ceramic International, 42(7),* 8431-8437. doi: 10.1016/j.ceramint.2016.02.062
15. Sembiring S., Riyanto A., Situmeang R., Sembiring Z. (2019): Bituminous Composite Comprising Amorphous Silica from Rice Husks. *Ceramics-Silikáty*, *63 (3)*, 277-286. doi: 10.13168/cs.2019.0021
16. Sembiring S., Riyanto A., Situmeang R., Sembiring Z., Susanti N., Firdaus I. (2020): Effect of amorphous rice husk silica addition on the structure of asphalt composite. *Metals Materials and Minerals*, *30 (4),* 113-118. doi: 10.14456/jmmm.2020.59
17. Sembiring S., Simanjuntak W., Manurung P., Asmi D., Low IM. (2014): Synthesis and characterization of gel-derived mullite precursors from rice husk silica. *Ceramic International, 40 (5),* 7067-7072. doi: 10.1016/j.ceramint.2013.12.038
18. Shen Y., Zhao P., Shao Q. (2014): Porous silica and carbon derived materials from rice husk pyrolysis char review. *Micropore and Mesopore Material, 4*, 188: 46-76. doi: 10.1016/j.micromeso.2014.01.005
19. Pode R. (2016): Potential applications of rice husk ash waste from rice husk biomass power plant. *Renewable and Sustainable Energy Reviews, 53*, 1468-1485. doi: 10.1016/j.rser.2015.09.051
20. Shen, Y. (2017): Rice husk silica derived nano-materials for sustainable applications. *Renewable and Sustainable Energy Reviews, 80*, 453-466. doi: 10.1016/j.rser.2017.05.115
21. Keller M., Fung J., Leion H., Mattisson T. (2016): Cu-impregnated alumina/silica bed materials for chemical looping reforming of biomass gasification gas. *Fuel, 180*, 448-456.
22. Shen Y., Wang J., Ge X., Chen M. (2016): By-products recycling for syngas cleanup in biomass pyrolysis – an overview. *Renewable and Sustainable Energy, 59*, 1246-1268. doi: 10.1016/j.rser.2016.01.077
23. Song Y., Che J., Zhang Y. (2011): The interacting rule of diatomite and asphalt groups. *Petroleum Science and Technology, 29 (3)*, 254-259. doi: 10.1080/10916460902882768
24. Cong P. L, Chen S. F, Chen H. X. (2012): Effects of diatomite on the properties of asphalt binder. *Construction and Building Material, 30*, 495-499. doi: 10.1016/j.conbuildmat.2011.11.011
25. Mojtaba G., Morteza M. S. Majid T., Jalal K. R. Reza T. (2012): Modification of stone matrix asphalt with nano-SiO_2. *Journal of Basic Applied Science Research, 2(2)*, 1338-1344.
26. Saram S. (2015): Impact of nano materials on rheological and physical properties of asphalt cement. American institute of science. *International Journal of Advanced Material Research, 1(1)*, 8-14.
27. Yao H., You Z., Li L., Lee C. H. Wingard D., Yap Y. K. Shi X., Goh S. W. (2013): Rheological properties and chemical bonding of asphalt modified with nanosilica. *Journal of Material Civil Engineering, 25(11)*, 1619-1630. doi: 10.1061/(ASCE)MT.1943-5533.0000690
28. Ezzat H., El-Badawy S., Gabr A., El-Saaid Ibrahim Z., Breakah T. (2016): Evaluation of Asphalt Binders Modified with Nanoclay and Nanosilica. *Procedia Engineering, 143*, 1260-1267. doi: 10.1016/j.proeng.2016.06.119
29. Baldi-Sevilla A., Montero M. L, Aguiar J. P. (2016): Influence of nano silica and diatomite on the physiochemical and mechanical properties of the binder at unaged and oxidized conditions. *Construction and Building Material, 127,* 176-182. Doi: 10.1016/j.conbuildmat.2016.09.140
30. Tan Y. Q. Shan L.Y. Fang J. (2009): Anti-cracking mechanism of diatomite asphalt and diatomite asphalt mixture at low temperature. Southeast University, 25 (1), 74-78.
31. Enieb M., Diab A. (2017): Characteristics of asphalt binder and mixture containing nanosilica. *International Journal of Pavement Research and Technology*, *10*(2), 148-157. doi: 10.1016/j.ijprt.2016.11.009
32. Bala N., Kamaruddin I., Napiah M., Danlami N. (2017): Rheological and rutting evaluation of composite nanosilica/polyethylene modified bitumen. *Material Science and Engineering, 201;*012012. doi:10.1088/1757-899X/201/1/012012
33. Wu S. P. Pang L., Mo, L. T. Chen Y. C. Zhu G. Jj. (2009): Influence of aging on the evolution of structure, morphology and rheology of base and SBS modified bitumen. *Construction and Building Material,* 23 1005-1010. doi: 10.1016/j.conbuildmat.2008.05.004

34. Yildirim, Y. (2007): Polymer modified asphalt binders. *Construction Building Material, 21(1),* 66-72. doi: 10.1016/j.conbuildmat.2005.07.007
35. Peters S. (2010): Nanocellulose and microcellulose fibers for concrete, Transportation Research Record 2142, *Transportation Research Board*, Washington, DC, 25-28
36. Jaskula P., Marcin Stienss M., Szydlowski C. (2017): Effect of polymer fibers reinforcement on selected properties of asphalt mixtures. *Procedia Engineering, 172*, 441-448. doi: 10.1016/j.proeng.2017.02.026
37. Abiola O. S. Kupolati W. K, Sadiku E. R. Ndambuki J. M. (2014): Utilization of natural fiber as modifier in bituminous mixes: A review. *Construction and Building Material, 54*, 305-312. doi: 10.1016/j.conbuildmat.2013.12.037
38. Tileuberdi K. Ye Z. A. Ongarbaev B. K. Mansurov E. A. Tuleutaef, Akkazyn. (2013): Physical and mechanical characteristics of rubber-bitumen compounds. *Chemical and Material Engineering, 1(4),* 105-10. doi: 10.13189/cme.2013.010401
39. Brown S. F. Needham D. (2000): A study of cement modified bitumen emulsion mixture. *Association of Asphalt Paving Technologists, 69*, 92-21.
40. Zhang F., and Yu J. (2010): The research for high-performance SBR compound modified asphalt. *Construction and Building Materials, 24(3*), 410-418. doi: 10.1016/j.conbuildmat.2009.10.003
41. Shen J., Amikhanian S. N. Xiao F., Tang B. (2009): Influence of surface area and size of crumb rubber on high temperature properties of crumb rubber modified binders. *Construction and Building Material, 23 (1)*, 304-310. doi: 10.1016/j.conbuildmat.2007.12.005
42. Cao W. (2007): Study on properties of recycled tire rubber modified asphalt mixtures using dry process. *Construction and Building Materials, 21(5)*, 1011-1015. doi: 10.1016/j.conbuildmat.2006.02.004
43. Putman B. J., and Amirkhanian S. N. (2004): Utilization of waste fibers in stone matrix asphalt mixtures. *Resource Conservation Recycle, 42(3)*;, 265-274. doi: 10.1016/j.resconrec.2004.04.005
44. LeBaron P. C., Wang Z., Pinnavaia T. J. (1999): Polymer-layered silicate nanocomposites: an overview. *Applied Clay Science, 15(1-2)*, 11-29. doi: 10.1016/S0169-1317(99)00017-4
45. Ray S. S., Okamoto M. (2003): Polymer/layered silicate nanocomposites: a review from preparation to processing. *Program Polymer Science, 28(11)*, 1539-1641. doi: 10.1016/j.progpolymsci.2003.08.002
46. Australian Standard, Refractories and Refractory Material Physical Test Methods. (1989): The Determination of Density, Porosity and Water Adsorption. Australian Standard, 1774, 1-4.
47. JIS A 5908, (2003): Japanese Standard Association. Japanese Industrial Standard Particle Board JIS A 5908, Japanese Standard Association.
48. Zhang F., Yu J., Han J. (2011): Effects of thermal oxidative ageing on dynamic viscosity, TG/DTG, DTA and FTIR of SBS- and SBS/sulfur-modified asphalts. *Construction and Building Materials, 25(1)*, 129-137. doi: 10.1016/j.conbuildmat. 2010.06.048
49. Larsen D. O. Alessandrini J. L. Bosch A., and Cortizo M. S. (2009): Micro-structural and rheological characteristics of SBS-asphalt blends during their manufacturing. *Construction and Building Materials*, 23(8), 2769-2774. doi: 10.1016/j.conbuildmat.2009.03.008